THE JOURNAL OF PHYSICAL CHEMISTRY B

Article

pubs.acs.org/JPCB

Harnessing Nanoscale Confinement to Design Sterically Stable Vesicles of Specific Shapes via Self-Assembly

Fikret Aydin, Geetartha Uppaladadium, and Meenakshi Dutt*

Department of Chemical and Biochemical Engineering, Rutgers The State University of New Jersey, Piscataway, New Jersey 08854, United States

Supporting Information

ABSTRACT: We design sterically stable biocompatible vehicles with tunable shapes through the self-assembly of a binary mixture composed of amphiphilic molecular species, such as PEGylated lipids, and phospholipids under volumetric confinement. We use a molecular dynamics-based mesoscopic simulation technique called dissipative particle dynamics to resolve the aggregation dynamics, structure, and morphology of the hybrid aggregate. We examine the effect of confinement on the growth dynamics and shape of the hybrid aggregate, and demonstrate the formation of different morphologies, such as oblate and prolate shaped vesicles and bicelles. We perform these investigations by varying the degree of nanoscale confinement, for different relative concentrations of the species and the length of the functional groups. Results from our investigations can be used for the design and prediction of novel hybrid soft materials for applications requiring the encapsulation of therapeutic agents in micro- or nanofluidic channels.

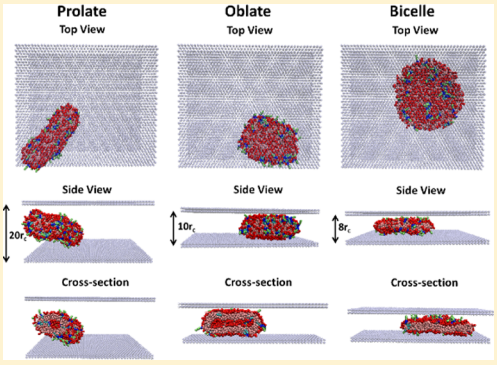

INTRODUCTION

Self-assembly of amphiphilic molecules in micro- and nanofluidic channels for the encapsulation of active compounds can be harnessed for applications in medical diagnostics and therapeutics.[1] The success of these approaches is critically dependent upon the ability of these molecules to assemble into aggregates of a desired morphology and dimension. One of the key challenges in the design of self-assembled nanostructured materials is the prediction of their resultant shape and size. The morphology of self-assembled structures can be controlled by either intrinsic factors such as molecular interactions, architecture, and composition or extrinsic factors such as the temperature, pH, and volume of the confinement.[2,3] Earlier studies have shown the size and geometry of the confining region to control the morphology of self-assembled materials on account of the increased local concentration, configurational frustration of the molecules, and interactions with the confining surfaces.[4,5] The dimensions, geometry, and surface selectivity of the confining environment have been found to strongly affect the self-assembled morphologies of block copolymers.[4,6−10] However, there remains a gap in our understanding of the role of the relative concentration of the molecular species, their molecular geometry, and the height of a slit-like confining volume on the structure and morphology of the aggregate.

The stability and shape of biocompatible carriers such as lipid vesicles influence the effective delivery of therapeutic agents to target cell populations.[11] A common route to designing sterically stable liposomes is via the grafting of poly ethylene glycol (PEG) chains to the lipid head groups.[12−14] In our previous study, we have demonstrated the design of a stable hairy vesicle composed of phospholipid and PEGylated lipid molecules via self-assembly, and identified the shape of the vesicle to be controlled by intrinsic factors[15] such as the molecular geometry and the relative concentration of the molecular species. In the present paper, we examine the self-assembly of two species of amphiphilic molecules with different interfacial areas, such as phospholipid and PEGylated lipid molecules, in a confined environment contained between two planar walls. We will study the structure and morphology of the binary component aggregate for different relative concentrations of the molecular species, their molecular geometry, and the height of the confining volume.

Earlier studies examining the self-assembly of block copolymers in confined regions have primarily used mean field theoretical approaches.[4,7−10,16] We have adopted a deterministic particle-based mesoscopic simulation technique entitled dissipative particle dynamics (DPD)[2,15,17−20] which simultaneously resolves both the molecular and continuum scales, for our investigations. The DPD method has been used to investigate the dynamics and morphology of self-assembly, phase separation, and phase transition in lipid systems,[21,22] block copolymers,[23] dense colloidal suspensions,[24] polymers in dilute solution or in a melt,[25] and chains in microfluidic channels.[26,27] Whereas the DPD method does not capture specific physical interactions such as electrostatics, these interactions can be effectively modeled via the use of suitable

Received: March 7, 2015
Revised: July 21, 2015
Published: July 24, 2015

DOI: 10.1021/acs.jpcb.5b02239
J. Phys. Chem. B 2015, 119, 10207−10215

soft repulsive interaction parameters. For example, the DPD simulation technique has been shown to capture the static and dynamic properties of bilayers composed of zwitterionic lipid molecules.[19,21]

Confinement induced microfluidic self-assembly can be used to produce lipid-polymeric nanoparticles for drug encapsulation or lipid-quantum dot nanoparticles for imaging purposes. This technique is advantageous compared to the conventional methods for the synthesis of multicomponent nanoparticles, since there are no additional steps like heating, vortexing, and long incubation times and the reproducibility of the particle size distribution is much higher by using microfluidic directed self-assembly.[1] Another application of microfluidic directed self-assembly is the formation of free-standing planar lipid membranes in the microfluidic channel. These membranes can be used to study membrane channel proteins for drug discovery, molecular sensing, and oligonucleotide analysis.[1] The production of high quality membrane is important to enable the measurement of host channel proteins at single-molecule conductance resolution.[1] In addition, confinement induced self-assembly of block copolymers can be used in various applications in nanotechnology such as nanolithography, fabrication of nanoporous membranes for advanced separation media, photonic crystals, high-density media storage, biomineralization, and drug delivery.[4] The impact of confinement can also be used to study shape transformations of red blood cells due to entropic contributions.[28]

Via self-assembly, we design binary vesicles encompassing hairy and nonhairy phospholipids under volumetric confinement, and examine the factors which can control the structure and morphology of the aggregates. Our results can potentially be used to design novel effective drug delivery vehicles in micro- and nanofluidic channels.

METHODOLOGY

DPD is a mesoscopic simulation technique that uses soft-sphere coarse-grained models to capture both the molecular details of the nanoscopic building blocks and their supramolecular organization while simultaneously resolving the hydrodynamics of the system over extended time scales.[2,20,29] In order to capture the dynamics of the soft spheres, the DPD technique integrates Newton's equation of motion via the use of similar numerical integrators used in other deterministic particle-based simulation methods.[20,30] The force acting on a soft sphere i due to its interactions with a neighboring soft sphere j ($j \neq i$) has three components: a conservative force, a dissipative force, and a random force, which operate within a certain cutoff distance r_c from the reference particle i. These forces are pairwise additive and yield the total force acting on particle i, which is given by $\mathbf{F}_i = \sum_{j\neq i} \mathbf{F}_{c,ij} + \mathbf{F}_{d,ij} + \mathbf{F}_{r,ij}$. The soft spheres interact via a soft-repulsive force ($\mathbf{F}_{c,ij} = a_{ij}(1 - (r_{ij}/r_c))\hat{\mathbf{r}}_{ij}$, for $r_{ij} < r_c$, and $\mathbf{F}_{c,ij} = 0$, for $r_{ij} \geq r_c$), a dissipative force ($\mathbf{F}_{d,ij} = -\gamma\omega^d(r_{ij})(\hat{\mathbf{r}}_{ij}\cdot\mathbf{v}_{ij})\hat{\mathbf{r}}_{ij}$), and a random force ($\mathbf{F}_{r,ij} = -\sigma\omega^r(r_{ij})\theta_{ij}\hat{\mathbf{r}}_{ij}$), where $\omega^d(r) = [w^r(r)]^2 = (1 - r)^2$ (for $r \geq 1$), $\omega^d(r) = [w^r(r)]^2 = 0$ (for $r \geq 1$), and $\sigma^2 = 2\gamma k_B T$. a_{ij} is the maximum repulsion between spheres i and j, $\mathbf{v}_{ij} = \mathbf{v}_i - \mathbf{v}_j$ is the relative velocity of the two spheres, $\mathbf{r}_{ij} = \mathbf{r}_i - \mathbf{r}_j$, $r_{ij} = |\mathbf{r}_i - \mathbf{r}_j|$, $\hat{\mathbf{r}}_{ij} = \mathbf{r}_{ij}/r_{ij}$, $r = r_{ij}/r_c$, γ is the viscosity related parameter used in the simulations, σ is the noise amplitude, $\theta_{ij}(t)$ is a randomly fluctuating variable from Gaussian statistics, and ω^d and ω^r are the separation dependent weight functions which become zero at distances greater than or equal to the cutoff distance r_c. Since the local linear and angular momentum is conserved by all three of these forces, even the small systems exhibit hydrodynamic behavior.[20] The constraints imposed on the random and dissipative forces by certain relations ensure that the statistical mechanics of the system conforms to the canonical ensemble.[20,30] The relation between the pair repulsion parameter a_{ij} and the Flory interaction parameter χ for a bead number density $\rho = 3r_c^{-3}$ is given by $\chi = (0.286 \pm 0.002)(a_{ij} - a_{ii})$.[20]

As shown in Figure 1a, the individual phospholipid molecules are represented by bead−spring models, and are modeled by a headgroup comprised of three hydrophilic beads and two hydrocarbon tails represented by three hydrophobic beads each. The hairy lipids, as shown in Figure 1b−d, encompass an identical architecture for the phospholipid, with hydrophilic tethers grafted to one of the hydrophilic head beads. The hairs or tethers are modeled by three, five, and six hydrophilic beads. Two consecutive beads in a chain are connected via a bond that is described by the harmonic spring potential $E_{bond} = K_{bond}((r - b)/r_c)^2$, where K_{bond} is the bond constant and b is the equilibrium bond length. The constants K_{bond} and b are assigned values of 64ε and $0.5r_c$, respectively.[2,17] The three-body stiffness potential along the lipid tails has the form $E_{angle} = K_{angle}(1 + \cos\theta)$, where θ is the angle formed by three adjacent beads. The coefficient K_{angle} is set to be 20ε in our simulations. The three-body stiffness term increases the stability and bending rigidity of the bilayers. Similar bond and angle potential functional forms and parameters are used for the tethers.

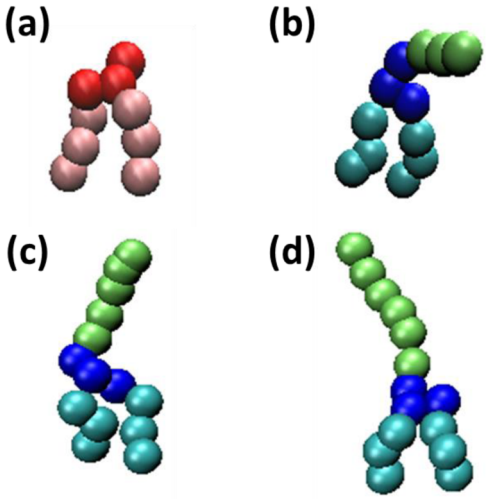

Figure 1. Images of the (a) amphiphilic phospholipid molecule, (b) hairy lipid molecule with a tether composed of three beads, (c) hairy lipid molecule with a tether composed of five beads, and (d) hairy lipid molecule with a tether composed of six beads.

Two planar walls parallel to the xy plane are used to confine the phospholipid and hairy lipid molecules, as shown in Figure 2a. The solvent molecules are present in the regions both between and above the walls. Each wall consists of two layers of frozen DPD particles, with a thickness given by $0.85r_c$ and a total area of $1779r_c^2$. The beads comprising the walls are organized in a triangular lattice.

In this paper, we illustrate the role of nanoscale confinement on the shape of self-assembled hairy vesicles encompassing phospholipid and hairy lipid molecules. Experimental examples of the hairs are polyethylene glycol chains with degrees of polymerization n given by 6, 10, and 12. We select these values

DOI: 10.1021/acs.jpcb.5b02239
J. Phys. Chem. B 2015, 119, 10207−10215

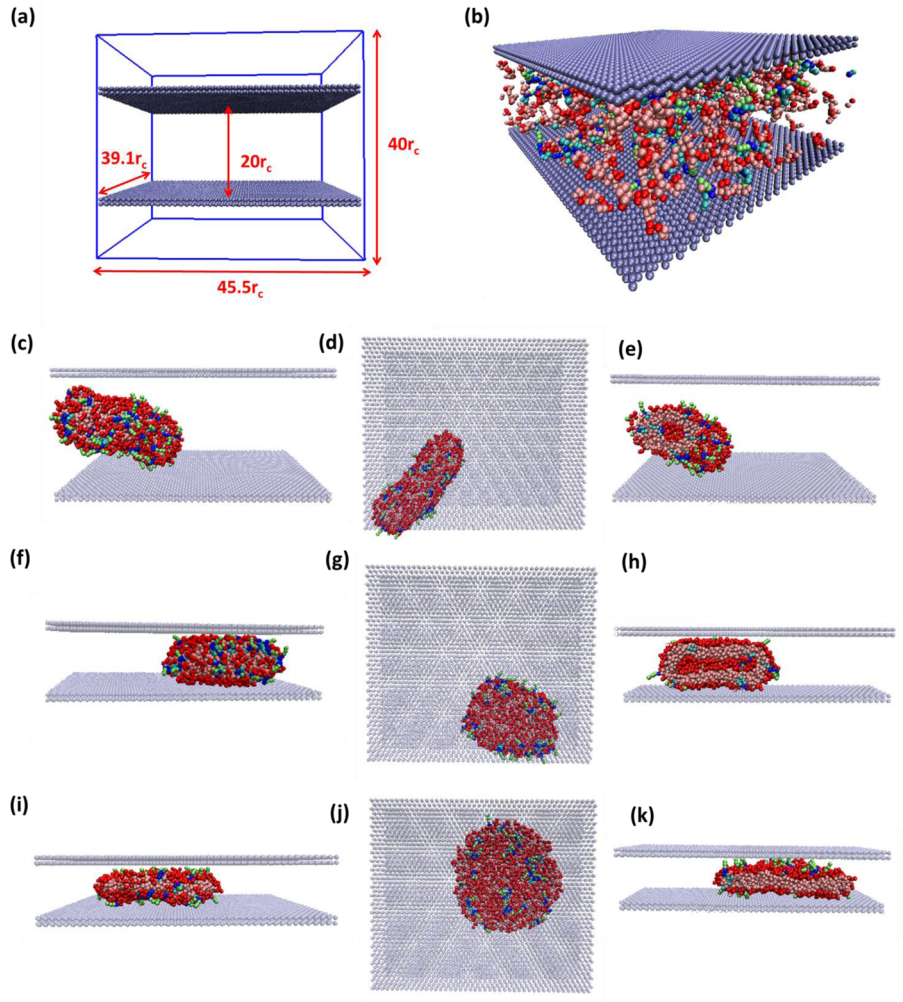

Figure 2. (a) The dimensions of the three-dimensional simulation box and channel used to confine the amphiphilic molecules. (b) The initial system configuration for a mixture of phospholipid and hairy lipid molecules in the confinement with a channel height of $15r_c$. (c) A side, (d) top, and (e) cross-sectional view of a self-assembled prolate vesicle in the confinement with a channel height of $20r_c$ at time $t = 120\,000\tau$. (f) A side, (g) top, and (h) cross-sectional view of a self-assembled oblate vesicle in the confinement with a channel height of $10r_c$ at time $t = 120\,000\tau$. (i) A side, (j) top, and (k) cross-sectional view of a self-assembled bicelle in the confinement with a channel height of $8r_c$ at time $t = 120\,000\tau$. The systems in parts b–k are composed of phospholipids (90%) and hairy lipid molecules with tethers composed of three beads (10%). The wall beads are reduced in size to enhance the top view of the different vesicle morphologies.

of the degree of polymerization to design sterically stabilized hairy vesicles with relatively short polyethylene glycol chains. In addition, earlier theoretical[31] and experimental studies[32,33] show polymers with 6–17 EO units to be sufficiently effective for reducing the amount of protein adsorption on a surface at a certain surface coverage. We examine the role of the height of the confining volume on the shape of the self-assembled hybrid aggregate, for different relative concentrations of the hairy lipids and lengths of the hairs.

The soft repulsive pair potential parameters for the lipid molecule head and tail beads were selected to capture its amphiphilic nature. In addition, the hair beads are considered to be hydrophilic in nature. To prevent the adhesion of the vesicle onto the surface of the wall, the wall beads are modeled to have favorable interactions with the solvent molecules and unfavorable interactions with the phospholipids and hairy lipids. An experimental analogy of the wall could be a hydrophilic surface with a charge distribution which results in unfavorable enthalpic interactions with the amphiphilic molecules.[34] Microfluidic channels can be made of materials such as glass, silicon, silicon oxide, and oxidized polystyrene. These materials can be sealed irreversibly with oxidized poly(dimethylsiloxane) (PDMS). The channel walls sealed with PDMS are found to be negatively charged in neutral and basic aqueous solutions.[35] It has been previously shown that vesicles composed of neutral and negatively charged lipid molecules, such as DOPC/DOPS, are not adsorbing onto the negatively charged silica surface.[36] The interaction parameters between the like components, a_{ij}, are based on the property of water.[20] The repulsion parameter between two beads of the same type is set at $a_{ii} = 25$ (measured in units of k_BT/r_c) which is based upon the compressibility of water at room temperature[20] for a bead density of $\rho = 3r_c^{-3}$. The soft repulsive interaction parameter a_{ij} between hydrophobic and hydrophilic beads is set at $a_{ij} = 100k_BT/r_c$, and is determined by using the Flory–Huggins interaction parameters, χ, as $a_{ij} = a_{ii} + 3.496\chi$, for $\rho = 3r_c^{-3}$.[20]

The soft repulsive interaction parameters between the tethers (T), head (h), and tail (t) beads of lipid types 1 and 2, the solvent (s) beads and the wall (w) beads are assigned the

DOI: 10.1021/acs.jpcb.5b02239
J. Phys. Chem. B 2015, 119, 10207–10215

following values (in units of k_BT/r_c): a_{ss} = 25, a_{TT} = 25, a_{Ts} = 25, a_{h1h1} = 25, a_{t1t1} = 25, a_{h2h2} = 25, a_{t2t2} = 25, a_{h1t1} = 100, a_{h1s} = 25, a_{t1s} = 100, a_{h2t2} = 100, a_{h2s} = 25, a_{t2s} = 100, a_{h1T} = 25, a_{t1T} = 100, a_{h2T} = 25, a_{t2T} = 100, a_{h1t2} = 100, a_{h2t1} = 100, a_{h1h2} = 25, a_{sw} = 25, a_{Tw} = 100, a_{h1w} = 100, a_{h2w} = 100, a_{t1w} = 100, and a_{t2w} = 100.

In our simulations, the respective characteristic length and energy scales are r_c and k_BT. As a result, our characteristic time scale can be described as $\tau = (mr_c^2/k_BT)^{1/2}$. Finally, σ = 3 and $\Delta t = 0.02\tau$ are used in the simulations along with the total bead number density of $\rho = 3r_c^{-3}$ and a dimensionless value of r_c = 1.[17] The mass of all the beads is set to unity.[2,17,19−21,29]

We draw a correspondence between our model and physical systems via the experimental properties of biological lipid bilayers.[29] The characteristic length scale is r_c = 0.76 nm, and is obtained through the comparison of experimental measurements of the interfacial area per lipid of a DPPC bilayer with similar measurements from our simulations. The time scale τ was calculated to be 6.0 ns by comparing the experimental measurement of the diffusion coefficient of a DPPC bilayer, which is given by 5×10^{-12} m^2/s,[17] with that obtained from the simulations. Using a temperature of 50 °C, the energy scale is calculated to be $\varepsilon = k_BT = 4.5 \times 10^{-21}$ J.

RESULTS AND DISCUSSION

a. Self-Assembly of Hairy Vesicle under Confinement.

We examine the self-assembly of hairy and nonhairy amphiphilic species in a confined volume bound by two rectangular planar walls, located in a simulation box of dimensions 45.5 × 39.1 × 40 r_c^3 with periodic boundaries along the three axes. The walls span the x and y dimensions of the simulation box, and are located at an equidistance from the origin of the simulation box, as shown in Figure 2a. The distance between their planar surfaces is varied from $8r_c$ to $20r_c$. The distance is chosen to effectively model different degrees of confinement. We use a 8:2, 8.5:1.5, and 9:1 binary mixture of phospholipid and hairy lipid molecules, with the hairs comprised of three, five, and six beads. Each system consists of 504 molecules. This corresponds to 50 hairy lipid molecules and 454 phospholipids for a 9:1 mixture, 76 hairy lipid molecules and 428 phospholipids for a 8.5:1.5 mixture, and 101 hairy lipid molecules and 403 phospholipids for a 8:2 mixture. We randomly place the molecules from each species in the confined volume between the two walls, as shown in Figure 2b. The solvent beads are both present between and above the two walls. We observe the formation of a single stable hairy vesicle via the self-assembly of the two species, as shown in Figure 2c. The self-assembly process is promoted by the unfavorable enthalpic interactions between the hydrophobic and hydrophilic species. The simulations are run for a time interval of 120 000τ. We observe the amphiphilic molecules to aggregate to form small clusters at the initial stages of the self-assembly process. This is followed by the formation of medium- to large-sized clusters via the diffusion, collision, and coalescence of the small clusters. We examine the role of the confining volume on the aggregation dynamics, for different hair lengths and relative concentrations of the two species. The relative concentration of the hairy lipids is set to 10, 15, and 20% for three different lengths of the hairs. The characterization presented in this paper uses particle trajectories from four simulations which have identical initial conditions but different random seeds.

We characterize the aggregation dynamics during the self-assembly process by measuring the scaling exponents of the time evolution of the number of clusters.[29] A cluster is defined to be a group of nonsolvent beads whose center-to-center distance is within the interaction cutoff distance which is given by r_c = 1. The number of clusters is given by the relation $N(t) \sim Ct^{\alpha}$, where $N(t)$ is the number of clusters, C is a constant, t is time, and α is the scaling exponent. We observe the aggregation dynamics at the channel heights of $15r_c$ to be quite similar to the aggregation dynamics at the channel heights of $20r_c$, as shown in Figure 3. We also calculate the scaling exponents for

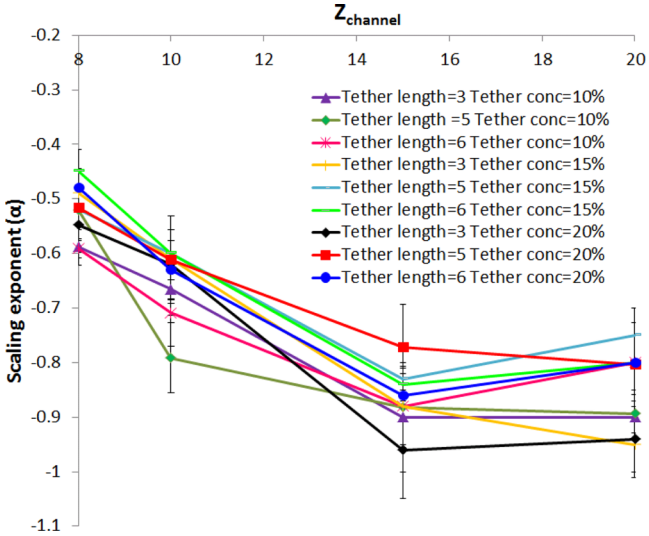

Figure 3. Plot of the scaling exponent α as a function of the distance between two planar surfaces for the self-assembly of binary mixtures composed of different relative concentrations of hairy lipid and phospholipid molecules, and length of the tethers.

the self-assembly in bulk conditions and find the results to be within 2−5% of the scaling exponents at the channel height of $20r_c$. This implies that confinement at the channel heights of $20r_c$ and $15r_c$ has negligible effects on the aggregation dynamics. The effect of the confinement on the aggregation dynamics has been observed when the channel height is reduced to $10r_c$ and $8r_c$. As the degree of confinement increases, the aggregation dynamics slows down, as evidenced from Figure 3. We surmise that increasing the degree of confinement results in greater steric hindrance between the small clusters encompassing phospholipids and hairy lipids. In addition, we expect the aggregation dynamics to slow down with an increase in the length of the tethers due to the higher steric hindrance and hydrodynamic drag. A possible explanation for the higher drag forces resulting from the longer hairs is the increase in the favorable enthalpic interactions between the longer chain-like functional groups and the solvent.[37,38] We demonstrate that the growth dynamics slows down with an increase in the length of tethers when the distance between two planar surfaces is $15r_c$ and $20r_c$, in line with our expectations. However, we do not observe the length of tethers to influence the growth dynamics as the degree of confinement increases. Our measurements demonstrate the growth dynamics to change negligibly with the relative concentration of the hairy lipids. We would like to note that our measurements of the scaling exponents for the lipids with the longer chain-like functional groups have been found to be in good agreement with similar measurements of the aggregation dynamics of phospholipid molecules and hairy nanotubes,[2] where the scaling exponent (α) has been reported

DOI: 10.1021/acs.jpcb.5b02239
J. Phys. Chem. B 2015, 119, 10207−10215

as ~ -0.8. We also measure the constant C in the relation $N(t) \sim Ct^{\alpha}$ in order to understand the effect of confinement on the aggregation dynamics at the initial stage of the self-assembly process. The duration of the initial stage of aggregation dynamics (prior to the measurement of scaling exponents) and the rate of aggregation dynamics at later stages (where the scaling exponent is measured) will affect the value of C. We expect a higher C value with a longer initial stage of aggregation dynamics where the individual molecules collide and coalescence to form small clusters. The value of C is also expected to increase with faster aggregation dynamics at later stages. As shown in Figure SI1, our measurements of the constant C as a function of the channel height and relative concentration of the hairy lipids for three different lengths of tethers are in agreement with our expectations. We demonstrate the value of C to increase with channel height and find its value in bulk conditions to be higher than that in the channel height of $20r_c$ ($C \sim 21\,000-23\,000$ for short tethers and $C \sim 14\,000-16\,000$ for long tethers). We surmise that the reason for higher values of C with decreasing confinement is the longer duration of the aggregation dynamics at the initial stage as longer time intervals are required for collision and coalescence encounters between the individual molecules. In addition, the scaling exponents at the channel height of $15r_c$ and $20r_c$ as well as in bulk conditions are indistinguishable, and do not show any increasing trends. Our results also show that the value of C decreases with longer tethers due to the slowdown in the aggregation dynamics.

b. Role of Confinement on the Morphology of the Self-Assembled Hairy Vesicles. The role of the volumetric confinement on the shape of the self-assembled structure can be gauged through measurements of the excluded volume of the chain-like functional groups, the reduced volume, the dimensions of the principal axes, the intermonolayer distribution of the hairy lipids, and the line tension. The excluded volume of the hairs in the monolayers can be measured through the radius of gyration, which is given by $R_g^2 = \lfloor \sum_{i=1,N+1} (\mathbf{r}_i - \mathbf{r}_{cm})^2 \rfloor / (N+1)$. $\mathbf{r}_i$ is the position vector of each bead in a hair, $\mathbf{r}_{cm}$ is the center-of-mass position of a hair, and N is the number of beads per hair. Following the formation of a single stable hairy vesicle, we calculate the radius of gyration of each hair in a given monolayer and average over all the hairs, as shown in Table 1. We find negligible differences in the radius of gyration for the short hairs (composed of three beads), indicating that they have enough space in the inner cavity of the vesicle to adopt fully extended conformational states. However, the intermonolayer asymmetry in the radius of gyration for the longer hairs (composed of five and six beads) shows the hairs to adjust their chain conformations to enable them to pack into the inner cavity of the vesicle. The excluded volume of the hairs will be shown to influence the distribution of the hairy lipids. The shape of the vesicle can be characterized through the reduced volume.

The reduced volume of the self-assembled hairy vesicles quantifies the degree of deviation from a spherical morphology and is given by[39] $\upsilon \equiv V/((4\pi/3)R^3)$, where V is the volume of the vesicle and R is the radius of the sphere with the same area as a vesicle with surface area A, given by $R \equiv (A/4\pi)^{1/2}$. In order to determine the surface area of the vesicles, we first map the coordinates of the head beads in the outer monolayer onto prolate and oblate ellipsoids, and then obtain all three elliptic radii to calculate the surface area of the ellipsoids. Our measurements of the reduced volume, as shown in Figure 4,

Table 1. Radius of Gyration of the Tethers Present in the Inner and Outer Monolayers of the Self-Assembled Vesicles for Different Relative Concentrations of the Hairy Lipids and Tether Lengths in the Confinement with a Channel Height of $10r_c$, $15r_c$, and $20r_c$

	conc. (%)	radius of gyration in the inner monolayer (r_c)	radius of gyration in the outer monolayer (r_c)
tether length = 3	10	0.43 ± 0.01	0.43 ± 0.02
$Z_{channel} = 10r_c$	15	0.41 ± 0.02	0.42 ± 0.01
	20	0.42 ± 0.01	0.44 ± 0.02
tether length = 5	10	0.59 ± 0.06	0.72 ± 0.02
$Z_{channel} = 10r_c$	15	0.59 ± 0.06	0.73 ± 0.02
	20	0.58 ± 0.04	0.74 ± 0.02
tether length = 6	10	0.73 ± 0.07	0.89 ± 0.03
$Z_{channel} = 10r_c$	15	0.72 ± 0.07	0.87 ± 0.03
tether length = 3	10	0.40 ± 0.03	0.41 ± 0.02
$Z_{channel} = 15r_c$	15	0.40 ± 0.03	0.43 ± 0.01
	20	0.42 ± 0.02	0.42 ± 0.01
tether length = 5	10	0.63 ± 0.04	0.71 ± 0.03
$Z_{channel} = 15r_c$	15	0.61 ± 0.04	0.70 ± 0.03
	20	0.64 ± 0.04	0.71 ± 0.02
tether length = 6	10	0.74 ± 0.06	0.84 ± 0.04
$Z_{channel} = 15r_c$	15	0.71 ± 0.05	0.87 ± 0.02
	20	0.74 ± 0.04	0.84 ± 0.04
tether length = 3	10	0.40 ± 0.01	0.43 ± 0.01
$Z_{channel} = 20r_c$	15	0.41 ± 0.02	0.43 ± 0.01
	20	0.40 ± 0.01	0.42 ± 0.01
tether length = 5	10	0.64 ± 0.05	0.71 ± 0.03
$Z_{channel} = 20r_c$	15	0.61 ± 0.03	0.70 ± 0.01
	20	0.64 ± 0.04	0.70 ± 0.02
tether length = 6	10	0.78 ± 0.04	0.83 ± 0.02
$Z_{channel} = 20r_c$	15	0.72 ± 0.05	0.85 ± 0.04
	20	0.72 ± 0.05	0.84 ± 0.02

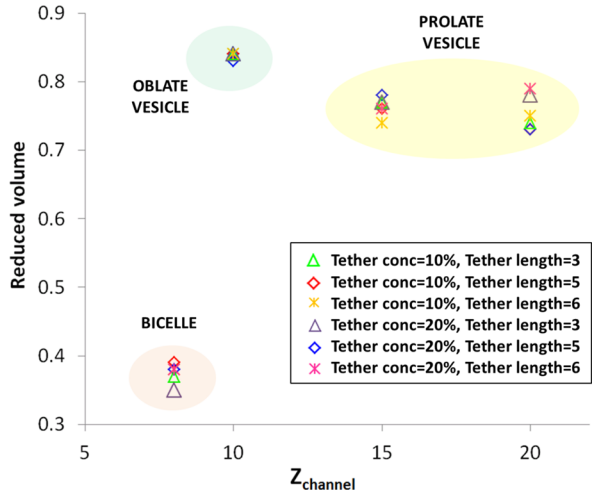

Figure 4. Plot of the reduced volume of the self-assembled hairy vesicles as a function of the distance between two planar surfaces for different relative concentrations of the hairy lipids and tether lengths.

demonstrate the shapes of the vesicles to deviate significantly from a spherical morphology ($\upsilon = 1$) and adopt either prolate and oblate shapes or bicelles depending on the degree of confinement during the self-assembly of the hairy vesicles. The results for the tether concentration of 15% are not shown in the figure, as they are very similar to the results for the tether concentrations of 10 and 20%. Our findings show that the self-

DOI: 10.1021/acs.jpcb.5b02239
J. Phys. Chem. B 2015, 119, 10207−10215

assembly of the phospholipid and hairy lipid molecules favors the formation of cigar-shaped (prolate) vesicles for various relative concentrations of the hairy lipids and the length of the hairs when the distance between the planar surfaces is set to $15r_c$ or $20r_c$. The corresponding reduced volumes of prolate vesicles are found to be within the range 0.7−0.8. The side, top, and cross-sectional views of the prolate vesicles are shown in Figure 2c−e, respectively. To understand the role of volumetric confinement on the reduced volume, we examine the self-assembly of phospholipid and hairy lipid molecules in the absence of the confining walls (by using the same relative concentrations of the hairy lipids and the length of the hairs). Our results for the reduced volume, as shown in Figure SI2, indicate the formation of hairy vesicles which have a very similar morphology to the vesicles in a confined region with heights of $15r_c$ and $20r_c$. We conclude the self-assembled morphology to be similar to that obtained in the bulk phase at these degrees of confinement. In order to increase the effect of the confinement, we set the distance between the planar surfaces to $10r_c$, and repeat the simulations examining the self-assembly of the phospholipid and hairy lipid molecules. An increase in the degree of confinement is found to favor the formation of disc-shaped (oblate) hairy vesicles, as captured by the side, top, and cross-sectional views, respectively, in Figure 2f−h. The corresponding reduced volumes of oblate vesicles are found to be within the range 0.8−0.9. This result indicates a shape transformation of the hairy vesicles from prolate to oblate shape with an increase in the degree of confinement. We surmise that, for sufficiently large distances between the planar walls, the prolate shape of the vesicle allows the self-assembled aggregate to maximize its rotational entropy about principal axes which are parallel or perpendicular to the planar walls. With a reduction in the separation distance between the walls, the vesicle maximizes its rotational entropy by adopting an oblate shape which enables rotation about a principal axis perpendicular to the plane of the walls. The shape transformation from a prolate to an oblate shape has been theoretically shown in a previous study[28] via the use of the area difference elasticity model (ADE). Helal et al.[28] investigated the stability of prolate and oblate shaped vesicles in a two-dimensional slit or one-dimensional cylinder by varying the degree of confinement. Although the reduced volumes for the prolate shaped vesicles are in good agreement with the model ($v_{prolate} > 0.65$), the reduced volumes for the oblate vesicles were measured to be higher than those for prolate vesicles, contrary to their findings ($v_{oblate} < 0.65$). This might be due to the fact that the self-assembly of vesicles, under the confinement, did not preserve the total volume or area of the membrane on account of the intermonolayer asymmetric distribution of the hairy lipids, as shown in Figure SI3. We would like to note that Helal et al. use preconfigured vesicle shapes and fixed enclosed volume and total area of the membrane. In addition, they do not include the thermal fluctuations of the bilayer in their model. Further reduction in the separation distance between the planar walls (to $8r_c$) results in a stable bicellar morphology, as captured by the side, top, and cross-sectional views, respectively, in Figure 2 i−k. The corresponding reduced volumes of bicelles are found to be within the range 0.3−0.4. These results demonstrate that the morphology of the self-assembled vesicles can be finely tuned by harnessing suitable confinement conditions. These findings enable the design of stable hairy vesicles with a well-defined shape and low polydispersity for applications such as liposomal drug delivery and gene therapy.[40,41]

The shape of the vesicle can also be characterized through the measurement of the principal axes[5] of the resulting aggregates and the projections along the axes (through the mapping of the coordinates of the head beads in the outer monolayer onto an ellipsoid,[42] as shown in Figure SI4). In order to find the principal axes, the algebraic expression of the ellipsoid is formed in the matrix of the quadratic form. The ellipsoid is centered in the Cartesian coordinate system by first finding its center and then forming its corresponding translation matrix. The translation matrix can be used to determine the principal axes by solving the eigenvalue problem. We compute the projections along the principal axes of the self-assembled hairy vesicles both with and without volumetric confinement, for different relative concentrations of the hairy lipids, the length of the hairs, and the distance between the surfaces of the walls. These results are shown in Table 2 (for channel heights of $8r_c$, $10r_c$, $15r_c$, and $20r_c$) and in Figure SI2 (for bulk conditions). Our measurements of the principal axes

Table 2. *x*, *y*, and *z* Principal Axes of the Self-Assembled Hairy Vesicles for Different Relative Concentrations of the Hairy Lipids and Tether Lengths in the Confinement with a Channel Height of $8r_c$, $10r_c$, $15r_c$, and $20r_c$

	conc. (%)	*x*-axis (r_c)	*y*-axis (r_c)	*z*-axis (r_c)
tether length = 3	10	16 ± 1	13 ± 1	2.0 ± 0.1
$Z_{channel} = 8r_c$	15	16 ± 1	14 ± 1	2.0 ± 0.1
	20	16 ± 1	14 ± 1	2.0 ± 0.1
tether length = 5	10	15 ± 1	13 ± 1	2.1 ± 0.2
$Z_{channel} = 8r_c$	15	15 ± 1	13 ± 1	2.1 ± 0.2
	20	15 ± 1	13 ± 1	2.1 ± 0.1
tether length = 6	10	15 ± 1	13 ± 1	2.1 ± 0.1
$Z_{channel} = 8r_c$	15	15 ± 1	13 ± 1	2.1 ± 0.2
	20	15 ± 1	13 ± 1	2.1 ± 0.2
tether length = 3	10	10 ± 1	8.1 ± 0.4	4.2 ± 0.1
$Z_{channel} = 10r_c$	15	11 ± 2	7 ± 1	4.2 ± 0.1
	20	10 ± 1	8.2 ± 0.4	4.2 ± 0.1
tether length = 5	10	10 ± 1	8.0 ± 0.4	4.2 ± 0.1
$Z_{channel} = 10r_c$	15	10 ± 1	8.0 ± 0.5	4.2 ± 0.1
	20	11 ± 1	7.8 ± 0.6	4.2 ± 0.1
tether length = 6	10	10 ± 1	7.9 ± 0.5	4.2 ± 0.1
$Z_{channel} = 10r_c$	15	10 ± 1	8.1 ± 0.4	4.2 ± 0.1
tether length = 3	10	15 ± 1	5.4 ± 0.3	4.5 ± 0.2
$Z_{channel} = 15r_c$	15	15 ± 1	5.4 ± 0.3	4.5 ± 0.2
	20	15 ± 1	5.4 ± 0.3	4.6 ± 0.2
tether length = 5	10	15 ± 1	5.4 ± 0.3	4.5 ± 0.2
$Z_{channel} = 15r_c$	15	16 ± 1	5.3 ± 0.3	4.4 ± 0.2
	20	15 ± 1	5.4 ± 0.3	4.6 ± 0.2
tether length = 6	10	16 ± 1	5.3 ± 0.4	4.3 ± 0.1
$Z_{channel} = 15r_c$	15	16 ± 1	5.3 ± 0.3	4.4 ± 0.2
	20	15 ± 1	5.4 ± 0.3	4.5 ± 0.1
tether length = 3	10	16 ± 1	5.4 ± 0.4	4.4 ± 0.2
$Z_{channel} = 20r_c$	15	16 ± 1	5.4 ± 0.4	4.4 ± 0.2
	20	15 ± 1	5.4 ± 0.3	4.6 ± 0.2
tether length = 5	10	16 ± 2	5.3 ± 0.4	4.4 ± 0.2
$Z_{channel} = 20r_c$	15	16 ± 2	5.4 ± 0.4	4.4 ± 0.2
	20	16 ± 1	5.4 ± 0.4	4.4 ± 0.2
tether length = 6	10	16 ± 1	5.4 ± 0.4	4.4 ± 0.2
$Z_{channel} = 20r_c$	15	14 ± 1	5.6 ± 0.2	4.7 ± 0.1
	20	14 ± 1	5.5 ± 0.3	4.7 ± 0.2

DOI: 10.1021/acs.jpcb.5b02239
J. Phys. Chem. B 2015, 119, 10207−10215

are consistent with our previous observations; the self-assembled hairy vesicles in the bulk and in channels of heights $15r_c$ and $20r_c$ have prolate shapes, whereas the self-assembled hairy vesicles in a channel with a height of $10r_c$ have oblate shapes. In addition, the self-assembled bicelles in a channel height of $8r_c$ have disc-shaped morphology but they have longer x and y dimensions and shorter z dimension, compared to the dimensions of oblate vesicles present in a channel with a height of $10r_c$. As shown in Table 2 and Figure SI2, the least variation in the vesicle dimensions is observed along the z-axis which coincides with the direction of confinement. We find that shape fluctuations due to the hydrodynamics and thermal fluctuations can be reduced by increasing the degree of confinement, as is evidenced from the standard deviations of the projections along the principal axes.

Our results illustrate an asymmetric distribution of the hairy lipid molecules in the two monolayers, as shown in Table 3.

Table 3. Number of Hairy Lipid Molecules Present in the Inner and Outer Monolayers of the Self-Assembled Vesicles for Different Relative Concentrations of the Hairy Lipids and Tether Lengths at Different Degrees of Confinement

	conc. (%)	number of tethers in the inner monolayer	number of tethers in the outer monolayer
tether length = 3	10	7 ± 1	43 ± 1
$Z_{channel} = 10r_c$	15	12 ± 4	64 ± 4
	20	17 ± 1	84 ± 1
tether length = 5	10	6	44
$Z_{channel} = 10r_c$	15	6 ± 1	70 ± 1
	20	7	94
tether length = 6	10	5	45
$Z_{channel} = 10r_c$	15	4	72
tether length = 3	10	5 ± 1	45 ± 1
$Z_{channel} = 15r_c$	15	11 ± 2	65 ± 2
	20	14 ± 2	87 ± 2
tether length = 5	10	4 ± 1	46 ± 1
$Z_{channel} = 15r_c$	15	7 ± 3	69 ± 3
	20	9 ± 1	92 ± 1
tether length = 6	10	2 ± 1	48± 1
$Z_{channel} = 15r_c$	15	5 ± 2	71 ± 2
	20	4 ± 1	97 ± 1
tether length = 3	10	9 ± 1	41 ± 1
$Z_{channel} = 20r_c$	15	10 ± 2	66 ± 2
	20	17 ± 1	84 ± 1
tether length = 5	10	5 ± 1	45 ± 1
$Z_{channel} = 20r_c$	15	5 ± 2	71 ± 2
	20	9 ± 2	92 ± 2
tether length = 6	10	3 ± 1	47 ± 1
$Z_{channel} = 20r_c$	15	8	68
	20	7 ± 1	94 ± 1

The asymmetry in the intermonolayer distribution is found to increase with the length of the hairs. These findings identify the parameters which can tune the intermonolayer distribution of the hairy lipids in the design of sterically stable vehicles to enable the storage of active compounds in the vesicle inner cavity.

We study the influence of the relative concentration of the hairy lipids, the length of the hairs, and the height of the confined region on thermodynamic variables such as the interfacial line tension. The line tension can be measured through the calculation of the excess free energy per unit length along the interface,[43] and is given by the following equation:[29,44] $\lambda \equiv [1/2(U_{AA} + U_{BB}) - U_{AB}]/l_{mo}$. U_{AA}, U_{BB}, and U_{AB} are the pair interaction energies between components A (hairy lipid molecules) and B (phospholipids), and l_{mo} is the average lateral size of the phospholipids and the hairy lipid molecules. We report the line tension to decrease with increasing relative concentration of the hairy lipids, as shown in Figure 5, and find this result to be in good agreement with an

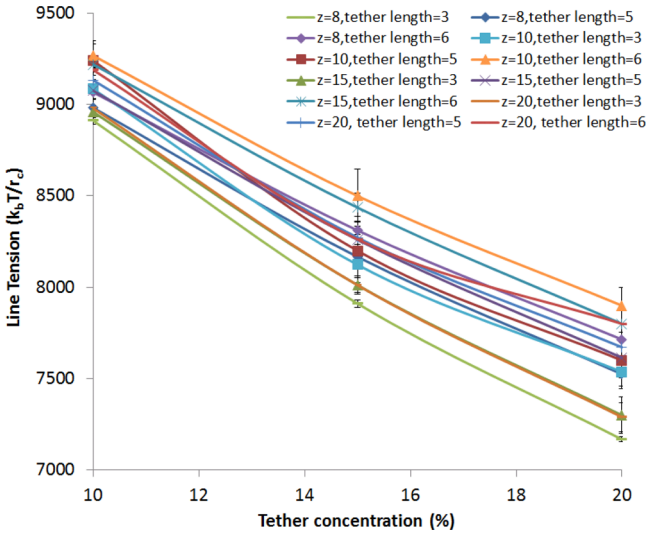

Figure 5. Plot of interfacial line tension of the self-assembled hairy vesicles as a function of tether concentration for different distances between two planar surfaces and different tether lengths.

earlier computational study.[45] A possible explanation for this observation could be the reduced interactions between the hairy lipids due to the excluded volume of the hairs. We also observe a small increase in the line tension with the length of the hairs. This observation can be explained by the increased mixing between the phospholipid and the hairy lipid molecules with higher excluded volume of the hairs, and therefore a larger pair interaction energy between the two molecular species. We do not observe the line tension of the self-assembled hairy vesicles to be influenced by the height of the confinement.

CONCLUSIONS

In summary, we have demonstrated the effects of nanoscale confinement on the shape of self-assembled hairy vesicles composed of phospholipid and PEGylated lipid molecules. Our results demonstrate the self-assembled hairy vesicles to have a prolate shape for different relative concentrations of the hairy lipids and the length of the hairs under bulk conditions, and volumetric confinement with channel heights of $15r_c$ and $20r_c$. As the degree of confinement increases (to channel heights of $10r_c$), the prolate shaped vesicles transform into an oblate shape for different relative concentrations of the hairy lipids and the length of the hairs. We find our observations to be in good agreement with earlier theoretical investigations that demonstrate oblate vesicles to be increasingly favored over prolate vesicles as the degree of confinement increases.[28] For a higher degree of confinement, we report the formation of stable bicellar structures. Contrary to expectations, we failed to observe a slowing down in the aggregation dynamics with increasing concentration of the hairy lipid molecules. For lipids with long hairs, the aggregation dynamics was observed to slow

DOI: 10.1021/acs.jpcb.5b02239
J. Phys. Chem. B 2015, 119, 10207−10215

down with the degree of confinement due to the increased hydrodynamic drag and steric hindrance of the tethers. We report an intermonolayer asymmetric distribution of the hairy lipids, along with differences in the excluded volume of the hairs with increasing length due to the volume constraints of the inner cavity of the vesicle. In addition, we observe the line tension to decrease with higher relative concentrations of the hairy lipids. A possible explanation of the decrease in the interfacial line tension is the reduced interactions between the hairy lipids due to the excluded volume of the tethers, as demonstrated by an earlier computational study.[45] Our results can be used to design therapeutic carriers with precisely tunable morphologies through the use of suitable nanoscale volumetric confinements, for longer circulation times and easy internalization by target cell populations.

■ ASSOCIATED CONTENT

Supporting Information

The Supporting Information is available free of charge on the ACS Publications website at DOI: 10.1021/acs.jpcb.5b02239.

A figure showing the constant C in the scaling exponent relation as a function of the channel height and relative concentration of the hairy lipids for three different lengths of tethers, a table showing the x, y, and z principal axes of the self-assembled hairy vesicles for different relative concentrations of the hairy lipids and tether lengths in bulk conditions (without walls), a table showing the total outer surface area and enclosed volume of the self-assembled hairy vesicles for different relative concentrations of the hairy lipids and tether lengths at different degrees of confinement, and a representative image showing the principal axes (x, y, and z) of the self-assembled binary prolate shaped hairy vesicle (PDF)

■ AUTHOR INFORMATION

Corresponding Author

*E-mail: meenakshi.dutt@rutgers.edu.

Notes

The authors declare no competing financial interest.

■ ACKNOWLEDGMENTS

The authors would like to acknowledge the use of high performance computational resources at the Rutgers Discovery Informatics Institute (http://rdi2.rutgers.edu/).

■ REFERENCES

(1) Khoo, H. S.; Lin, C.; Huang, S.-H.; Tseng, F.-G. Self-Assembly in Micro- and Nanofluidic Devices: A Review of Recent Efforts. *Micromachines* **2011**, *2*, 17−48.

(2) Dutt, M.; Kuksenok, O.; Nayhouse, M. J.; Little, S. R.; Balazs, A. C. Modeling the Self-Assembly of Lipids and Nanotubes in Solution: Forming Vesicles and Bicelles with Transmembrane Nanotube Channels. *ACS Nano* **2011**, *5*, 4769−4782.

(3) Dutt, M.; Kuksenok, O.; Balazs, A. C. Designing Tunable Bionanostructured Materials via Self-assembly of Amphiphilic Lipids and Functionalized Nanotubes. *MRS Online Proc. Libr.* **2012**, *1464*, 1471.

(4) Shi, A.-C.; Li, B. Self-Assembly of Diblock Copolymers Under Confinement. *Soft Matter* **2013**, *9*, 1398−1413.

(5) Li, X.; Tang, Y.-H.; Liang, H.; Karniadakis, G. E. Large-Scale Dissipative Particle Dynamics Simulations of Self-Assembled Amphiphilic Systems. *Chem. Commun.* **2014**, *50*, 8306−8308.

(6) Stewart-Sloan, C. R.; Thomas, E. L. Interplay of Symmetries of Block Polymers and Confining Geometries. *Eur. Polym. J.* **2011**, *47*, 630−646.

(7) Sushko, M. L.; Liu, J. Surfactant Two-Dimensional Self-Assembly under Confinement. *J. Phys. Chem. B* **2011**, *115*, 4322−4328.

(8) Bianchi, E.; Likos, C. N.; Kahl, G. Self-assembly of Heterogeneously Charged Particles under Confinement. *ACS Nano* **2013**, *7*, 4657−4667.

(9) Yang, G.; Tang, P.; Yang, Y.; Cabral, J. T. Self-assembly of AB Diblock Copolymers under Confinement into Topographically Patterned Surfaces. *J. Phys. Chem. B* **2009**, *113*, 14052−14061.

(10) Wang, Z.; Li, B.; Jin, Q.; Ding, D.; Shi, A.-C. Self-Assembly of Cylinder-Forming ABA Triblock Copolymers under Cylindrical Confinement. *Macromol. Theory Simul.* **2008**, *17*, 301−312.

(11) Kolhar, P.; Anselmo, A. C.; Gupta, V.; Pant, K.; Prabhakarpandian, B.; Ruoslahti, E.; Mitragotri, S. Using Shape Effects to Target Antibody-Coated Nanoparticles to Lung and Brain Endothelium. *Proc. Natl. Acad. Sci. U. S. A.* **2013**, *110*, 10753−10758.

(12) Rex, S.; Zuckermann, M. J.; Lafleur, M.; Silvius, J. R. Experimental and Monte Carlo Simulation Studies of the Thermodynamics of Polyethyleneglycol Chains Grafted to Lipid Bilayers. *Biophys. J.* **1998**, *75*, 2900−2914.

(13) Szleifer, I.; Gerasimov, O. V.; Thompson, D. H. Spontaneous Liposome Formation Induced by Grafted Poly (Ethylene Oxide) Layers: Theoretical Prediction and Experimental Verification. *Proc. Natl. Acad. Sci. U. S. A.* **1998**, *95*, 1032−1037.

(14) Nicholas, A. R.; Scott, M. J.; Kennedy, N. I.; Jones, M. N. Effect of Grafted Polyethylene Glycol (PEG) on the Size, Encapsulation Efficiency and Permeability of Vesicles. *Biochim. Biophys. Acta, Biomembr.* **2000**, *1463*, 167−178.

(15) Aydin, F.; Uppaladadium, G.; Dutt, M. Design of Shape-tunable Hairy Vesicles. *Colloids Surf., B* **2015**, *128*, 268−275.

(16) Li, W.; Wickham, R. A. Self-Assembled Morphologies of a Diblock Copolymer Melt Confined in a Cylindrical Nanopore. *Macromolecules* **2006**, *39*, 8492−8498.

(17) Smith, K. A.; Jasnow, D.; Balazs, A. C. Designing Synthetic Vesicles that Engulf Nanoscopic Particles. *J. Chem. Phys.* **2007**, *127*, 084703.

(18) Laradji, M.; Sunil Kumar, P. B. Dynamics of Domain Growth in Self-assembled Fluid Vesicles. *Phys. Rev. Lett.* **2004**, *93*, 198105.

(19) Illya, G.; Lipowsky, R.; Shillcock, J. C. Two-component Membrane Material Properties and Domain Formation from Dissipative Particle Dynamics. *J. Chem. Phys.* **2006**, *125*, 114710−114719.

(20) Groot, R. D.; Warren, P. B. Dissipative Particle Dynamics: Bridging the Gap between Atomistic and Mesoscopic Simulation. *J. Chem. Phys.* **1997**, *107*, 4423−4435.

(21) Kranenburg, M.; Venturoli, M.; Smit, B. Phase Behavior and Induced Interdigitation in Bilayers Studied with Dissipative Particle Dynamics. *J. Phys. Chem. B* **2003**, *107*, 11491−11501.

(22) Yamamoto, S.; Maruyama, Y.; Hyodo, S. Dissipative Particle Dynamics Study of Spontaneous Vesicle Formation of Amphiphilic Molecules. *J. Chem. Phys.* **2002**, *116*, 5842−5849.

(23) Chou, S. H.; Tsao, H. K.; Sheng, Y. J. Morphologies of Multicompartment Micelles Formed by Triblock Copolymers. *J. Chem. Phys.* **2006**, *125*, 194903.

(24) Boek, E. S.; Coveney, P. V.; Lekkerkerker, H. N. W.; van der Schoot, P. Simulating Rheology of Dense Colloidal Suspensions Using Dissipative Particle Dynamics. *Phys. Rev. E: Stat. Phys., Plasmas, Fluids, Relat. Interdiscip. Top.* **1997**, *55*, 3124−3131.

(25) Spenley, N. A. Scaling Laws for Polymers in Dissipative Particle Dynamics. *Europhys. Lett.* **2000**, *49*, 534−540.

(26) Fan, X.; Phan-Thien, N.; Chen, S.; Wu, X.; Ng, T. Y. Simulating Flow of DNA Suspension Using Dissipative Particle Dynamics. *Phys. Fluids* **2006**, *18*, 063102−063110.

(27) Chen, S.; Phan-Thien, N.; Fan, X.-J.; Khoo, B. C. Dissipative Particle Dynamics of Polymer Drops in Periodic Shear Flow. *J. Non-Newtonian Fluid Mech.* **2004**, *118*, 65−81.

DOI: 10.1021/acs.jpcb.5b02239
J. Phys. Chem. B 2015, 119, 10207−10215

(28) Helal, K.; Biben, T.; Hansen, J.-P. Influence of Capillary Confinement on the Equilibrium Shape of Vesicles. *J. Phys.: Condens. Matter* **1999**, *11*, 51−58.
(29) Aydin, F.; Ludford, P.; Dutt, M. Phase Segregation in Bio-inspired Multi-component Vesicles Encompassing Double Tail Phospholipid Species. *Soft Matter* **2014**, *10*, 6096−6108.
(30) Allen, M. P.; Tildesley, D. J. *Computer Simulations of Liquids*; Clarendon Press: Oxford, U.K., 2001.
(31) Satulovsky, J.; Carignano, M. A.; Szleifer, I. Kinetic and Thermodynamic Control of Protein Adsorption. *Proc. Natl. Acad. Sci. U. S. A.* **2000**, *97*, 9037−9041.
(32) Prime, K. L.; Whitesides, G. M. Self-assembled Organic Monolayers: Model Systems for Studying Adsorption of Proteins at Surfaces. *Science* **1991**, *252*, 1164−1167.
(33) Prime, K. L.; Whitesides, G. M. Adsorption of Proteins onto Surfaces Containing End-Attached Oligo (ethylene oxide): A Model System Using Self-Assembled Monolayers. *J. Am. Chem. Soc.* **1993**, *115*, 10714−10721.
(34) Kim, P.; Lee, S. E.; Jung, H. S.; Lee, H. Y.; Kawai, T.; Suh, K. Y. Soft Lithographic Patterning of Supported Lipid Bilayers onto a Surface and inside Microfluidic Channels. *Lab Chip* **2006**, *6*, 54−59.
(35) Duffy, D. C.; McDonald, J. C.; Schueller, O. J.; Whitesides, G. M. Rapid Prototyping of Microfluidic Systems in Poly-(dimethylsiloxane). *Anal. Chem.* **1998**, *70*, 4974−4984.
(36) Richter, R.; Mukhopadhyay, A.; Brisson, A. Pathways of Lipid Vesicle Deposition on Solid Surfaces: A Combined QCM-D and AFM Study. *Biophys. J.* **2003**, *85*, 3035−3047.
(37) Li, Y.; Zhang, X.; Cao, D. The Role of Shape Complementarity in the Protein-Protein Interactions. *Sci. Rep.* **2013**, *3*, 3271.
(38) Yang, K.; Vishnyakov, A.; Neimark, A. V. Polymer Translocation through a Nanopore: DPD Study. *J. Phys. Chem. B* **2013**, *117*, 3648−3658.
(39) Seifert, U.; Berndl, K.; Lipowsky, R. Shape Transformations of Vesicles: Phase Diagram for Spontaneous-curvature and Bilayer-coupling Models. *Phys. Rev. A: At., Mol., Opt. Phys.* **1991**, *44*, 1182.
(40) Hood, R. R.; Kendall, E. L.; Junqueira, M.; Vreeland, W. N.; Quezado, Z.; Finkel, J. C.; DeVoe, D. L. Microfluidic-Enabled Liposomes Elucidate Size-Dependent Transdermal Transport. *PLoS One* **2014**, *9*, 92978.
(41) Jahn, A.; Stavis, S. M.; Hong, J. S.; Vreeland, W. N.; DeVoe, D. L.; Gaitan, M. Microfluidic Mixing and the Formation of Nanoscale Lipid Vesicles. *ACS Nano* **2010**, *4*, 2077−2087.
(42) http://www.mathworks.com/matlabcentral/fileexchange/24693-ellipsoid-fit (accessed Nov 12, 2014).
(43) Weijs, J. H.; Marchand, A.; Andreotti, B.; Lohse, D.; Snoeijer, J. H. Origin of Line Tension for a Lennard-Jones Nanodroplet. *Phys. Fluids* **2011**, *23*, 022001−022011.
(44) Lipowsky, R.; Dimova, R. Domains in Membranes and Vesicles. *J. Phys.: Condens. Matter* **2003**, *15*, 31−45.
(45) Shinoda, W.; Discher, D. E.; Klein, M. L.; Loverde, S. M. Probing the Structure of PEGylated-Lipid Assemblies by Coarse-grained Molecular Dynamics. *Soft Matter* **2013**, *9*, 11549−11556.

DOI: 10.1021/acs.jpcb.5b02239
J. Phys. Chem. B 2015, 119, 10207−10215